




Article

Hydrogen Peroxide Promotes the Production of Radiation-Derived EVs Containing Mitochondrial Proteins

Caitlin E. Miller¹, Fangfang Xu¹, Yanming Zhao¹, Wei Luo², Weixiong Zhong³, Kristy Meyer³, Rani Jayswal⁴, Heidi L. Weiss⁴, William H. St. Clair², Daret K. St. Clair¹ and Luksana Chaiswing^{1,*} 

¹ Department of Toxicology and Cancer Biology, University of Kentucky, Lexington, KY 40506, USA

² Department of Radiation Medicine, University of Kentucky, Lexington, KY 40506, USA

³ Department of Pathology and Laboratory Medicine, University of Wisconsin-Madison, Madison, WI 53706, USA

⁴ Biostatistics Shared Resource Facility, Markey Cancer Center, University of Kentucky, Lexington, KY 40506, USA

* Correspondence: l.chaiswing@uky.edu; Tel.: +1-859-218-3407

Abstract: In spite of extensive successes, cancer recurrence after radiation treatment (RT) remains one of the significant challenges in the cure of localized prostate cancer (PCa). This study focuses on elucidating a novel adaptive response to RT that could contribute to cancer recurrence. Here, we used PC3 cell line, an adenocarcinoma from a bone metastasis and radio-resistant clone 695 cell line, which survived after total radiation dose of 66 Gy (2 Gy × 33) and subsequently regrew in nude mice after exposure to fractionated radiation at 10 Gy (2 Gy × 5). Clone 695 cells not only showed an increase in surviving fraction post-radiation but also an increase in hydrogen peroxide (H₂O₂) production when compared to PC3 cells. At the single cell level, confocal microscope images coupled with IMARIS rendering software demonstrate an increase in mitochondrial mass and membrane potential in clone 695 cells. Utilizing the Seahorse XF96 instrument to investigate mitochondrial respiration, clone 695 cells demonstrated a higher basal Oxygen Consumption Rate (OCR), ATP-linked OCR, and proton leak compared to PC3 cells. The elevation of mitochondrial function in clone 695 cells is accompanied by an increase in mitochondrial H₂O₂ production. These data suggest that H₂O₂ could reprogram PCa's mitochondrial homeostasis, which allows the cancer to survive and regrow after RT. Upon exposure to RT, in addition to ROS production, we found that RT induces the release of extracellular vesicles (EVs) from PC3 cells ($p < 0.05$). Importantly, adding H₂O₂ to PC3 cells promotes EVs production in a dose-dependent manner and pre-treatment with polyethylene glycol-Catalase mitigates H₂O₂-mediated EV production. Both RT-derived EVs and H₂O₂-derived EVs carried higher levels of mitochondrial antioxidant proteins including, Peroxiredoxin 3, Glutathione Peroxidase 4 as well as mitochondrial-associated oxidative phosphorylation proteins. Significantly, adding isolated functional mitochondria 24 h prior to RT shows a significant increase in surviving fractions of PC3 cells ($p < 0.05$). Together, our findings reveal that H₂O₂ promotes the production of EVs carrying mitochondrial proteins and that functional mitochondria enhance cancer survival after RT.

Keywords: hydrogen peroxide; radiation resistance; mitochondria; extracellular vesicles



Citation: Miller, C.E.; Xu, F.; Zhao, Y.; Luo, W.; Zhong, W.; Meyer, K.; Jayswal, R.; Weiss, H.L.; St. Clair, W.H.; St. Clair, D.K.; et al. Hydrogen Peroxide Promotes the Production of Radiation-Derived EVs Containing Mitochondrial Proteins. *Antioxidants* **2022**, *11*, 2119. <https://doi.org/10.3390/antiox11112119>

Academic Editor: Mikko O. Laukkanen

Received: 29 August 2022

Accepted: 15 October 2022

Published: 27 October 2022

Publisher's Note: MDPI stays neutral with regard to jurisdictional claims in published maps and institutional affiliations.



Copyright: © 2022 by the authors. Licensee MDPI, Basel, Switzerland. This article is an open access article distributed under the terms and conditions of the Creative Commons Attribution (CC BY) license (<https://creativecommons.org/licenses/by/4.0/>).

1. Introduction

Prostate cancer (PCa) is one of the most diagnosed cancers in men besides skin cancer [1]. This cancer arises from the overgrowth of the epithelial lining within the prostate [2]. It is estimated that there will be around 268,490 cases diagnosed in the US in 2022 [3]. Not only is this cancer one of the most diagnosed in men, but it is the second leading cause of cancer death in men. It is estimated that 11% of male cancer deaths will be attributed to PCa. Both of these percentages have steadily increased over recent years [1,4,5]. Viable treatment options for prostate cancer include surgery, radiation, and hormone therapy [6].

Radiation is a widely used treatment for many cancers. Around 50% of PCa patients will receive radiation over the course of their treatment [7]. Radiation kills cancer cells via at least two mechanisms; (1) The direct effect, by directly causing ionization of macromolecules and (2) indirect effect, by producing reactive oxygen species (ROS) such as the superoxide anion, hydroxy anion, and H₂O₂ through radiolysis of water [8,9]. ROS production specifically within the mitochondria can further stimulate ROS production by increasing mitochondria membrane permeability [9]. The ROS produced by the indirect effect can also cause DNA breaks, further damaging the cell through increasing mitochondrial membrane permeability, causing protein misfolding, and lipid peroxidation [9,10]. Due to tumor heterogeneity, it is difficult for radiation to target every cell within these tumors. Although a widely used treatment, some cases of PCa will recur after radiation. For the purpose of our study, this will be called radiation resistance. The mitochondrial-mediated mechanism of how these cancers become resistant is debated. Some argue that alterations in mitochondria can lead to radiation sensitivity, while others conclude that mitochondria can contribute to radiation resistance [11,12].

H₂O₂ is one of the ROS that is produced during radiation treatment (RT) [9]. H₂O₂ possesses a longer half-life (2.2 s versus 10⁻⁶ and 10⁻⁹ s) compared to the other ROS produced during radiation treatment [13–17]. This information in combination with the ability to diffuse with the utilization of aquaporin proteins, makes H₂O₂ a viable signaling molecule causing cascades throughout the cell via oxidation of proteins [18]. In normal tissue, H₂O₂ is used for physiological responses such as metabolism, cell proliferation, and immune cell recruitment [19]. Although necessary for normal physiological functions, when the concentration of H₂O₂ is too high (>100 nM), it can disrupt redox signaling, causing pathophysiology [19]. In cancer, this increased amount of H₂O₂ can lead to cancer metabolism and metastasis [20,21].

Mitochondria are arguably the most important organelle within a cell. They are known for their involvement in making ATP using the tricarboxylic acid cycle (TCA) and the electron transport chain (ETC). These organelles are implicated in many other important processes such as cell death, immunological responses, and radiation-induced signaling [22]. Although necessary for cellular function, mitochondria also have implications in many pathologies [23]. Under physiological conditions, ROS are mostly produced at complexes I and III of the ETC [24,25]. These ROS can further damage the mitochondria by causing protein and lipid oxidation within them, as well as outside of the mitochondria [9,26]. Cells can increase their mitochondrial mass using fission/fusion processes during mitochondrial biogenesis [27]. Although this is thought of as the main pathway of increasing mitochondria, there is a novel process called mitochondrial transfer in which mitochondrial particles or pieces are transferred from cell to cell. This can happen in a variety of ways such as tunneling nanotubing, dendritic transfer, naked mitochondrial particles, and extracellular vesicles [28,29].

Extracellular vesicles (EV) are membrane bound particles that can carry cargo from cell to cell. These particles come in three main forms, exosomes, microvesicles, and apoptotic bodies. These subtypes differ in their size, route of generation, and markers on the membrane. Exosomes are generated by the intake of the limited multivesicular body, which is then released into the extracellular environment. Microvesicles are formed by the budding of the cellular plasma membrane. Lastly, apoptotic bodies are formed when the cell is undergoing apoptosis and releasing their contents [30–33]. Extracellular vesicles can carry a wide variety of cargo, including RNA, mitochondria and mitochondrial contents [34–37]. Cargos of EVs have been proposed to use as a non-invasive tool for the detection, characterization, and monitoring of cancer such as prostate cancer. Proteo-transcriptomic analyses of EVs from serum of patients reveal enrichment of RNA-proteins, RNA-RNA complexes, and markers which are exclusively expressed in prostate tissues [38]. Additionally, recent study by Chen Tzu-Yi et al. demonstrated that mitochondrial inner membrane proteins are the EV enriched protein signatures that are not significantly different from their cancer cell of origin, implicating a coordinated mechanism between EVs and their donor cells [39].

Cancer reprogramming is an adaptive response mechanism(s) that contributes to cancer survival and progression; including rewired cellular redox state, up-regulated metabolism, as well as activated mitochondrial biogenesis. Our laboratory demonstrated that carboplatin

resistant ovarian cancer cells have higher mitochondria function and H_2O_2 production levels than the parental ovarian cells [40] while aggressive PCa tissues exhibited redox imbalances via ROS-mediated post-translational modifications of antioxidant enzymes [41]. Previous studies have shown that ROS are generated during RT [42]. Due to the fact that radiation can cause the production of H_2O_2 , we generated our radioresistant cell line, Clone 695. We measured the amount of H_2O_2 produced in Clone 695 cells that survived radiation treatment (both in vivo and in vitro), compared to the parental PCa cell line (PC3 cells). As anticipated, mitochondrial parameters such as mitochondrial respiration, mitochondrial mass, and mitochondrial membrane potential are increased in radioresistant PCa cells. Significantly, we observed EV production upon RT, including EVs carrying mitochondrial contents. In this study, we sought to (1) determine if EVs containing mitochondria is a novel mechanism that contributes to cancer reprogramming via elevated mitochondrial function in PCa cells that survive RT and (2) if H_2O_2 could be an arbitrator upon radiation-mediated EV production.

2. Materials and Methods

2.1. Cell Culture

PC3 cells and PC3 cells that survived radiation treatment (RR-PCa called “Clone 695”) were grown in 5% CO_2 conditions at 37 C in RPMI-1640 supplemented with 1% glutamine, 10% FBS, Hepes, 1% sodium Pyruvate, and 1% penicillin/streptomycin antibiotics. Tissue culture reagents were purchased from Sigma and Gibco. Cells were passaged less than 10 times. PC3 cells (cat.CRL-1435, ATCC, Manassas, VA, USA) were purchased from ATCC. Cell authentication of Clone 695 cells was completed by ATCC using the Cell line Authentication Sample Collection Kit and Service (cat. 70049374) (Supplementary Figure S1).

2.2. Radioresistant Prostate Cancer Cell (Clone 695) Development

PC3 cells were irradiated at 2 Gy/day, 5 times per week, and allowed to rest on the weekends. This process was performed until the total dosage was 66 Gy. Cells that survived 66 Gy radiation were then subcutaneously injected into athymic nude mice. Animal experimental procedures were approved by the Institutional Animal Care and Use Committee of the University of Kentucky (Lexington, KY, USA), approval Protocol No. 01077M2006. Once tumors reached 200–250 mm^3 in size measured by a caliper (3 times a week), they were irradiated at 2 Gy daily until the total dosage was 10 Gy, which is the dose that suppresses tumor growth established previously in the lab [43]. TrueBeam Varian Linear accelerator (6 MeV) was used for animal radiation (Varian Medical System Inc., Palo Alto, Santa Clara, CA, USA). After about two months, tumors regrew in 2 of the 10 mice (as shown in Figure 1A). These tumors were collected and isolated into a monolayer using a tumor digestion kit from Cell Biolabs INC (cat.CBA-155). Once monolayer cells were established, we performed a colony survival assay to confirm clone 695’s ability to survive radiation.

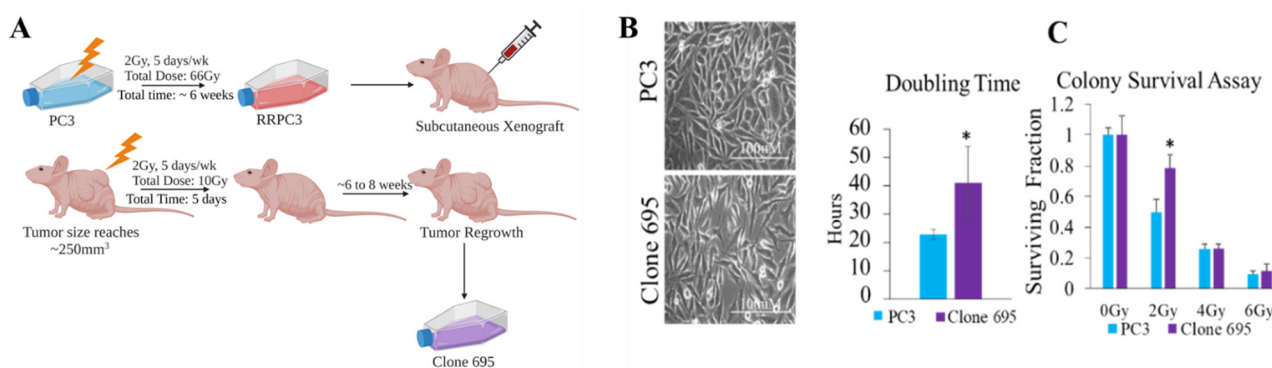


Figure 1. Distinct morphology and survival of Clone 695 cells compared to PC3 cells. (A) The process of clone 695 development. (B) Cell morphology and cell doubling times of PC3 and Clone 695 cell lines calculated from cell growth curve. (C) Colony survival assay of PC3 and Clone 695 cell lines after cells were irradiated at 0 Gy, 2 Gy, 4 Gy, or 6 Gy. * p -value < 0.05.

2.3. Cell Growth and Doubling Time Point

Cells were plated at 20,000 cells/well in a corning 12-well clear plate. Cells were collected using trypsin and counted at 24, 48, 72, and 96 h using a hemocytometer in conjunction with trypan blue and bright field microscope (10× magnification). The doubling time point was calculated as follows using the “cell calculator” tool (doubling-time.com; Roth v. 2006):

$$\text{Doubling Time} = \frac{\text{duration} \times \log(2)}{\log(\text{Final Concentration}) - \log(\text{Initial Concentration})}$$

2.4. Colony Survival Assay

Cells were plated in a corning 6-well clear plate at 100, 200, 300, and 500 cells per well for 0, 2, 4, and 6 Gy treatment, respectively. Cells were stained with crystal violet and 2.5% paraformaldehyde solution 10–13 days after treatment. Number of colonies was determined by counting colonies of 50 cells or greater. The Plating efficiency (PE) and surviving fraction (SF) were then calculated as follows [44]:

$$\text{PE} = \frac{\text{no. of colonies formed}}{\text{no. of cells seeded}} \times 100\%$$

$$\text{SF} = \frac{\text{no. of colonies formed after treatment}}{\text{no. of cells seeded XPE}}$$

2.5. EV Isolation

PC3 cells were plated at a concentration of 5×10^6 cells in a 15 cm corning dish and were irradiated with 0, 6, 46, or 66 Gy. Each dosage represented the following models: control (0 Gy), effect producing dosage (6 Gy), a mid-point to radiation resistant (46 Gy), and radiation resistant (66 Gy) models. The media was changed to media supplemented with 10% exosome free media from System Biosciences (Palo Alto, Santa Clara, CA, USA), 24 h prior to RT. Prior to EV isolation, media from cells was collected 72 h post treatment and filtered using 0.8 μM filter from lifesciences to remove cells and debris larger than 800 nm. Media collected was stored at -80°C . EVs were then isolated using the affinity-based method from the Qiagen Exoeasy kit (Germantown, MD, USA). The media collected was thawed and mixed with binding buffer at a 1:1 ratio. This mixture was added to the spin columns and spun at 500 g for 1 min. This process was repeated until all sample/buffer mixture was spun to allow EVs to bind to the column. Next, 10 mL of washing buffer was added to the columns and centrifuged at max (3095 \times g) for 5 min to rinse off any impurities. Lastly, the spin column was added to a fresh conical tube and 1 mL of elution buffer was added to the columns and spun at 500 g for 5 min. The eluate was then placed back onto the column and spun at max (3095 g) for 5 min. To concentrate isolated EVs, the samples were added to an Amicon ultra 3000 filter, which allowed molecules lower than 3 kDa to pass through (cat # UFC500396) in a volume of $\sim 450 \mu\text{L}$ and centrifuged for 50 min at 14,000 \times g. To collect the concentrated EVs, the 3000 filter was placed upside-down into a new centrifugal tube and spun at 14,000 \times g for 5 min.

2.6. EV Measurements

Concentration and size measurements were performed using the ZetaView Nanotracking Analyzer (Particle Metrics, Munich, Germany). Standard bead size of 110 nm was used for calibration prior to running the samples. Samples were diluted in ultrapure 1 \times PBS pH 7.4 (EV grade, Thermofisher, Waltham, MA, USA) that was filtered through a 0.2 μm PES filter at a 1:10,000 ratio (0.5 μL sample into 5 mL of EV grade PBS). Diluted samples were loaded at a volume of 1 mL. Rinsing was performed in between replicates and each sample with filtered 1 \times PBS.

2.7. Protein Expression by Capillary Based-Automated Western BLOT JESS

Isolated EVs were lysed by adding a lysis buffer containing 11 μL protease inhibitor, 11 μL EDTA, and 200 μL RIPA buffer at a 1:4 ratio. After adding EV lysis buffer, samples were sonicated for 30 s and placed on ice for one minute for three cycles. After the sonication process, samples were allowed to rest on ice for 30 min. Protein concentrations were obtained using the rapid gold bicinchoninic acid assay (ThermoFisher). Samples were then diluted with 0.1 \times sample buffer to yield 1 $\mu\text{g}/\mu\text{L}$ according to the Jess protocol provided by Protein Simple (San Jose, CA, USA). Briefly, samples were added with 5 \times fluorescent master mix, boiled, and loaded to the instrument at a 1 $\mu\text{g}/\mu\text{L}$ concentration. The following primary antibodies were used: Peroxiredoxin 3 (Prx3) (Proteintech, Rosemont, IL, USA), Transcription factor A, mitochondrial (TFAM) (Santa Cruz Biotechnology, Dallas, TX, USA), NADH Dehydrogenase 4 (ND4) (Abcam, Boston, MA, USA), Succinate dehydrogenase A (SDHA) (Proteintech), mitochondrial cytochrome bc1 Complex III (Proteintech), Thioredoxin Reductase 2 (TrxR2) (Proteintech), Nuclear factor erythroid 2-related factor 2 (Nrf2) (Abcam, Cambridge, UK) Manganese superoxide dismutase (MnSOD) (Upstate, Mt Upton, NY, USA), Catalase (Proteintech), Glutathione peroxidase 4 (GPx4) (Proteintech), and Flotilin-1 (Flot-1) (Novus, Centennial, CO, Centennial, CO, USA). All primary antibodies were used at a 1:20 dilution, unless specific. A chemiluminescent secondary detection system was used with either rabbit or mouse secondary antibodies (Protein Simple, San Jose, CA, USA).

2.8. Metabolic Parameters

For the mitochondrial stress test and glycolytic stress test, PC3 cells and Clone 695 cells were plated at 20,000 cells/well in a 96-well plate and either the Oxygen Consumption Rate (OCR) or the Extracellular Acidification Rate (ECAR) were obtained using the Seahorse XFe96 analyzer from Agilent. The mitochondrial stress test was performed by measuring the initial OCR followed by 1 μM of oligomycin to inhibit complex V (ATP Synthase) of oxidative phosphorylation. 1 μM of FCCP uncoupler was added to collapse the proton gradient followed by 1 μM of both rotenone and antimycin A to inhibit complexes I and III respectively. Spare Respiratory capacity was calculated from the subtraction of the basal OCR (prior to oligomycin treatment) from the maximal OCR (obtained after FCCP treatment). Lastly, ATP-linked OCR was obtained by subtracting the OCR subsequent to oligomycin treatment from the initial (basal) OCR. For the glycolytic stress test, 10 mM glucose is added to start the glycolysis process. Next, 1 μM of oligomycin was added to inhibit complex V. Lastly, 50 mM of 2-deoxyglucose was added to end the glycolytic process by competitively binding to glucose hexokinase. Glycolysis is measured by the ECAR post glucose-injection. The glycolytic capacity is determined by the ECAR after the addition of oligomycin [40].

To determine actual ATP production, an ADP/ATP ratio assay kit from Sigma was used (cat.MAK135-1KT). Cells were plated into a clear 96-well plate from Corning at a concentration of 5000 cells/well. Luminescent readings were taken using the SpectraMax Plus 384 from Molecular Devices.

To measure lactate production, 5000 cells/well were plated into a 96-well clear plate from Corning. The media was taken from these cells in a volume of 50 μL and placed into a 96-well plate. A lactate assay kit from Sigma Aldrich (St. Louis, MO, USA) (cat#MAK064) was used and absorbance readings were taken at 570 nm using the SpectraMax Plus 384 from Molecular Devices.

2.9. ROS Measurements

Measurement of H_2O_2 released into the media was performed using an Amplex Red kit from Thermo Fisher (Invitrogen, Waltham, MA, USA). Polyethylene glycol (PEG)-Catalase (cat.C4963-2MG) (PEG-Cat) as a negative control was added to the cells at a concentration of 500 U/ μL , 24 h prior to the measurement. A volume of 50 μL of media was transferred into another clear 96-well plate. Absorbance readings were taken using the SpectraMax Plus 384

at 560 nm 2 h after Amplex red reagent was added. Mitochondrial H₂O₂ production was measured using the fluorescent probe, MitoPY1 obtained from Biotechne (Minneapolis, MN, USA). MitoPY1 (50 µM) was added to the cells, protected from light, and incubated for 30 min. Cells were washed with PBS (3 times) and MitoPY1 media was replaced with phenol red free-RPMI media. Fluorescent intensity was measured at 495/515 nm using the spectra max plus 384 from molecular devices.

2.10. H₂O₂ Treatment

Cells were seeded (~2 × 10⁶ cells/plate) in a 75 cm² flask for 24 h. H₂O₂ was added in concentrations of 60, 120 and 240 µM for 24 h. Cells treatment with 500 Unit PEG-Cat were used as negative control. Cells and media were collected for further experiments including NTA analysis and Jess Automated Western Blot.

2.11. Mitochondrial Mass Measurements and IMARIS Software

PC3 cells were stained with Mitotracker Green FM (mitochondria, ThermoFisher, Waltham, MA, USA, Cat#M17514), cell mask red (cell membrane, Thermo Fisher Cat#A57245), and hoechst (nucleus, Thermo Fisher Cat#H3570). Images were then taken with the Nikon A1 confocal microscope using a Z-stack (Z range:10.00 µM, Step:1.00 µM). The images from the NIS-Element (v5; Nikon Instruments Inc. Melville, NY, USA) were converted into Imaris files (IMS format) by Imaris rendering software (v9.6; Oxford Instruments, Abingdon, UK) for 3D visualization and DATA processing. Border of each cell was traced based on cell mark fluorescence intensity. Green fluorescent intensity represents mitochondrial mass in each cell was then segmented and quantified based on automated relative fluorescence algorithm provided by Imaris software. The following parameters were collected: Green intensity mean per mitochondrion, volume per mitochondrion based on GFP, Sphericity of mitochondrion, and Ellipticity of mitochondrion.

2.12. Electron Microscopy

1. EV imaging

50 µg of EVs placed into PBS were mixed 1:1 with a 2% glutaraldehyde in freshly made sodium phosphate for a final concentration of 1% glutaraldehyde and fixed overnight at 4 °C. Fixed exosomes in a volume of 5 µL were placed on parafilm with the shiny side of the copper grid and allowed to absorb for 20 min. The grid was then washed twice with 100 µL of filtered water. Samples were then stained for 10 min in 2% Uranyl acetate (UA) in water. Excess stain was removed by touching the edge of the grid to filter paper and washing once with a drop of filtered water. Excess water was removed by touching the edge of the grid to filter paper and setting the grid shiny side up to dry. Lastly, the grid was observed under transmission electron microscopy at 80 kV [45].

2. Cell Imaging

Cells were grown on cover slip for 24 h following by 6 Gy RT. After 24 h post-RT, 2.5% glutaraldehyde fixative in Sorenson's phosphate buffer, pH 7.4 was placed onto the samples and fixed for 30 min. The glutaraldehyde was decanted and rinse 3 times, 5 min each, with room temperature Sorenson's phosphate buffer, pH 7.4. Post-fixing was performed by adding Caulfield's OsO₄ with sucrose for 30 min at room temperature. The samples were then rinsed with ddH₂O twice for 5 min each time. Dehydration was performed by adding tissue to a graded series of ethanol (15%, 30%, 50%, 75%, 95%, and 4 times of 100%) for 2 min each. Samples were then added to 100% propylene oxide twice for 5 min. Next, 100% EMBED 812 was added to blue flat-bottom moulds (Ted Pella Inc, Redding, CA, USA, Cat#10504), and sample (cells on cover slip) was added in the corner of the mould cell side up. Mould was then polymerized for 18 h in a 65 °C oven. Moulds and blocks were removed. Hydrofluoric acid (32%) was used to dissolve cover slip (30 min) [46]. Samples were then sectioned, stained with UA, and observed under a TEM.

2.13. Extracellular Vesicle Uptake

PC3 cells at 5000 cells/well were seeded in 24 well-black with glass bottom plate (0.170 ± 0.005 mm) (Cellvis, Mountain View, CA, USA, Catalog #P24-1.5H-N) and stained using hoechst (nucleus) and cell mask red (cell membrane). EVs were stained with exo-glow protein-EV labeling kit overnight and treated onto the cells at a concentration of 30 ug/time point. Images were taken using the Nikon-A1 microscope with a CO₂ chamber at 7 h and at 24 h after EV treatments.

2.14. Mitochondrial Treatment

Mitochondria were isolated from PC3 cells (1×10^6 cells) using mitochondrial isolation kit for cultured cells according to manufacturing protocol (Cat#89874, ThermoFisher). Isolated mitochondria (0 ug or 10 ug) were then added onto a separate set of PC3 cells using the mitoception method [47]. The plate was spun at 500 g for 5 min for accelerated mitochondrial uptake. After 24 h, excess mitochondria were removed. Cells were then treated with 2 Gy radiation daily (administered 3 times, total dosage 6 Gy) and colony survival assays were performed 10 days post-radiation. For fluorescence imaging, the mitochondria were stained with Mitotracker Red CMXRos to visualize the uptake of external isolated mitochondria.

2.15. Statistical Analysis

Data analyses and graphical displays were generated using GraphPad Prism or SAS 9.4. Pairwise comparisons of the mean difference(s) between the vehicle group and treatment group or cell lines was employed with an unpaired, two-sample *t*-test; while comparison of the 6 Gy treatment group normalized to 0 Gy values was performed using a one-sample *t*-test. Comparison means in more than two groups was accomplished using one-way ANOVA. A Turkey post hoc test was subsequently applied. *p*-value at ≤ 0.05 was assigned to be significant.

For analysis of particle counts as a function of diameter size and treatment, a generalized linear mixed model was utilized accounting for repeated diameter measurements within a sample and as well as random intercept for each sample. A negative binomial distribution was utilized to account for zero particle counts. Furthermore, the cube root of the particle counts (the outcome) was modelled with a third-degree polynomial function of the cube root of the particle diameter, the radiation/treatment groups and their interactions; testing for the significance of the interaction terms was performed to achieve a parsimonious model. The model curve in the final graph represents the predicted values for the outcome at each group and diameter combination. SAS version 9.4 was utilized for statistical modeling.

3. Results

3.1. Radioresistant PCa Cell Line Clone 695 Shows a Significant Difference in Morphology, Growth Rate, and Resistance to Radiation When Compared to Parental PC3 Cells

In order to elucidate the mechanism behind cancer survival and regrowth after RT (radiation resistant phenotype), we developed a PCa cell line named “clone 695”. This cell line was created using PC3 cells, an adenocarcinoma derived from bone metastasis PCa. These PC3 cells were irradiated at 2 Gy, 5 times a week until the total dosage was 66 Gy. Cells that survived this treatment regimen were continued to be cultured and maintained as described in Materials and Methods and were named radio-resistant PC3 cells (RRPC3 cells). Subsequently, RRPC3 cells were subcutaneously xenografted into nude mice. When tumor sizes reached around 250 mm³, the tumors were irradiated at 2 Gy/day until the total dosage was 10 Gy. Although tumors shrunk initially, after 6–8 weeks, some of the tumors regrew (2 out of 10). These tumors were collected, isolated into a monolayer cell line. We then named this cell line “clone 695” (Figure 1A). As shown in Figure 1B, the morphology of clone 695 cell line showed an elongated and fibroblast-like appearance while PC3 cells showed a shorter and more epithelial-like morphology (Figure 1B). Growth curve analysis

during log phase showed that clone 695 cells grow slower than PC3 cells with a doubling time point of 40 h (2 fold higher than PC3 cells) (Figure 1B). To confirm that clone 695 cells were more resistant to radiation than the parental PC3 cells, a colony survival assay was performed. These results showed that clone 695 had a higher surviving fraction than PC3 cells at a 2 Gy dosage (2 fold higher), which is a commonly administered dose in the clinic (Figure 1C). These findings suggest that clone 695 cells show a different phenotype from the parental PC3 cells.

3.2. Radioresistant PCa Cell Line Clone 695 Shows an Increase in Mitochondrial Mass in Individual Cells

When radiating PC3 cells into RRPC3 cells, around the 38 Gy treatment mark, granular structures were observed within the cells (Figure 2A). To further investigate this phenomenon, a mitotracker green fluorescent probe was used to stain the mitochondria within the cells. PC3 cells were either irradiated with sham (0 Gy) or radiation. Upon imaging, it was observed that there were the same structures observed in the cells under brightfield microscopy (Figure 2(A1,A2)), and these structures were stained positive with mitotracker green using a confocal microscope. These data suggest that the granulated structure within the PC3 cells during radiation resistant development are mitochondria (Figure 2(A3,A4)). Due to an increase in mitochondria observed during RT, we investigated whether clone 695 cells have a higher amount of mitochondrial mass than PC3 cells. Using mitotracker green, confocal images were taken of both PC3 and Clone 695 cell lines. After obtaining these images, they were converted into IMS format using a rendering software called IMARIS. By using automated algorithm, the software allows automated tracking, detection, segmentation and quantification analysis of mitochondria on a per cell basis (Supplementary Figure S3). A color-coded scale bar on the rendered images indicates the intensity of mitochondrial mass based on green fluorescent intensity (red = high, blue/purple = low) (Figure 2B). As shown in Figure 2C, it was observed that clone 695 cell line had an increase in segmented mitochondrial mass and volume per cell, when compared to PC3 cell line. Quantification data also suggests more spherical and elliptical (oblate) mitochondrion in clone 695 cells than PC3 cells (Figure 2C). Due to an increase in mitochondrial mass and volume, the redox status of Clone 695 cells was further investigated in comparison to PC3 cells.

3.3. Radioresistant PCa Cell Line Clone 695 Shows an Increase in H₂O₂ Production

Since RT is known to increase the level of ROS within the cell, the amount of H₂O₂ released into the media was measured using an Amplex red assay. As shown in Figure 3A, clone 695 cells had a significantly higher level of H₂O₂ released into the media than PC3 cells. Since ROS production correlates with mitochondrial electron transport chain, specifically mitochondrial membrane permeability, the mitochondrial membrane potential was measured using a TMRE fluorescence probe. Clone 695 cells showed a significantly higher mitochondrial membrane potential than PC3 cells (Figure 3B). To determine where this H₂O₂ was produced within the cell, a MitoPY1, a fluorescence probe that is specific to mitochondrial H₂O₂ was incubated with the cells (Figure 3C). It was found that clone 695 shows a significantly higher level of mitochondrial H₂O₂. This suggests that the increase in H₂O₂ within the cell is, at least in part, coming from the mitochondria.

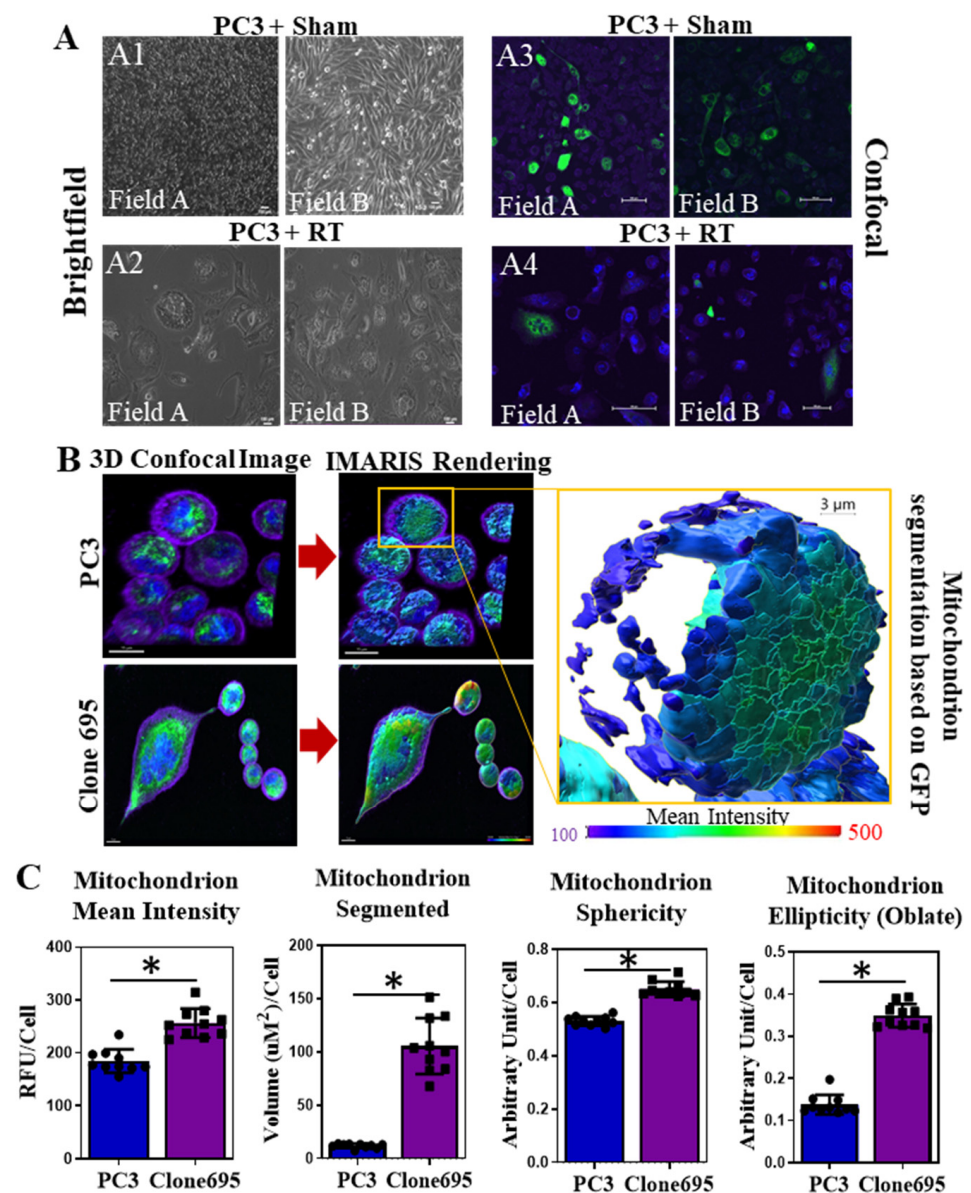


Figure 2. Clone 696 cells show distinct mitochondrial features compared to PC3 cells. (A) Cell morphology observed during PC3 cells treated with fractionated RT (clone 695 development). Cells that were exposed to RT altered their morphology with abundance mitochondria observed in cells with larger size. (A1) Brightfield images from two different fields and (A3) confocal images from two different fields, of PC3 cells taken at 0 Gy RT (sham). (A2) Brightfield images from two different fields and (A4) confocal images from two different fields, of PC3 cells after treated with 38 Gy RT. Scale bar = 100 μ m. Green = Mitochondria, Blue = Nucleus, Purple = membrane. (B) Confocal images of PC3 cells and Clone 695 cells converted into IMARIS file for visualization of segmented mitochondria in a single cell. Scale bar = 100 μ m. (C) Quantitative analysis of each mitochondrion segmented per cell for mitotracker green intensity, mitochondrial volume, mitochondrial sphericity and mitochondrial ellipticity, compared between PC3 cells and clone 695 cells. Circles and squares represent individual data points within PC3 and Clone 695 samples. * p -value < 0.01.

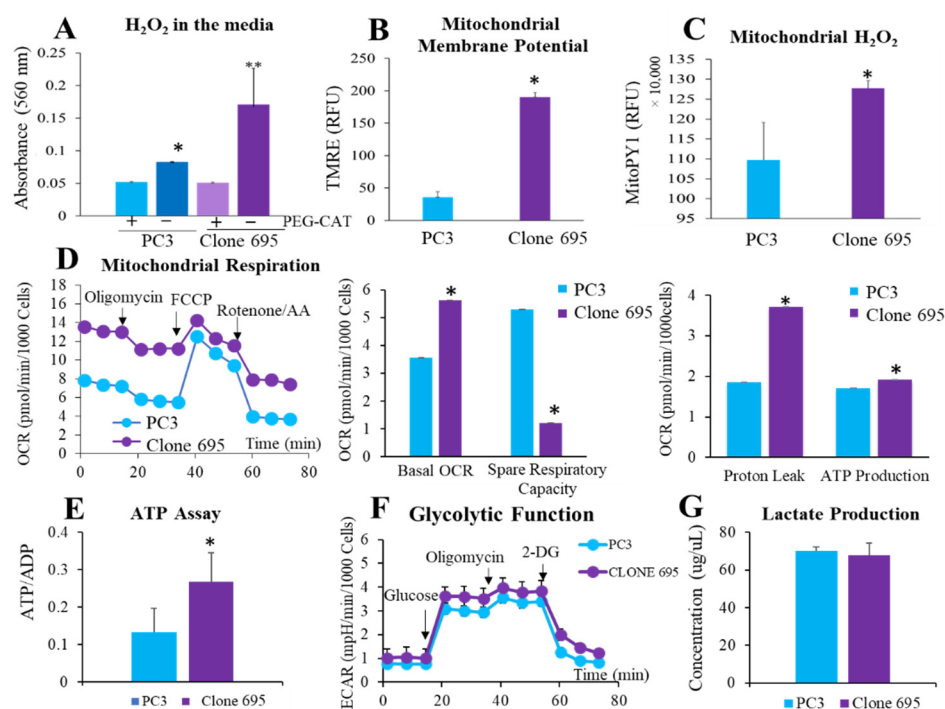


Figure 3. Clone 695 cells shows an increase in H₂O₂ production and mitochondrial respiration compared to PC3 cells. (A) H₂O₂ released into the media after 24 h incubation using an Amplex red assay. PEG-CAT (500 unit) was added for negative control. (B) TMRE staining shows mitochondrial membrane potential. (C) MitoPY1 intensity indicating mitochondrial H₂O₂ production. RFU = Relative fluorescence unit. (D) Seahorse Mitochondrial Stress Test. Respiration graphs calculated by response to inhibitors (oligomycin, FCCP, and Rotenone/Antimycin A (AA)). (E) ATP/ADP ratio kit showing ATP produced. (F) Seahorse Glycolytic stress test. Graph values calculated by response to inhibitors added during assay (Glucose, Oligomycin, and 2-DG). (G) Lactate Assay (measuring d-lactate). * *p*-value < 0.05, ** *p*-value < 0.09.

3.4. Elevation of Mitochondrial Respiratory Activity Correlates with Reprogramming of Mitochondrial Homeostasis in Radioresistant PCa Cell Line Clone 695

With an increase in mitochondrial H₂O₂ as well as mitochondrial membrane permeability, we further tested if there are the differences in mitochondrial respiratory activity between clone 695 cells and PC3 cells. In performing a Seahorse mitochondrial stress test, clone 695 cells show a higher basal OCR, proton leak, and ATP-linked OCR but not spare respiratory capacity, when compared to PC3 cells (Figure 3D). Although clone 695 cell line has a higher amount of ATP-linked OCR, however, this value is calculated on the OCR and is not an actual measurement of ATP. To measure actual ATP production, an ATP/ADP ratio kit was used. As shown in Figure 3E, clone 695 cell line has a higher ATP production than PC3 cells. To investigate if an increase in ATP mainly derived from the mitochondria, a glycolytic stress test was performed using Seahorse instrument. As shown in Figure 3F, ECAR levels in clone 695 cells were not significantly different from PC3 cells. In addition, clone 695 cells showed no difference in lactate production when compared to PC3 cells (Figure 3G). These data suggest that the increase in ATP production is derived from the processes within the mitochondria. Overall, these data imply energy metabolism reprogramming associated with an increase in mitochondrial mass and function in radioresistant PCa.

3.5. Extracellular Vesicles Are Released upon Radiation Treatment

Due to the significance of EVs as cargo carrier, we next tested if EVs were being produced upon RT. PC3 cells were irradiated with 6 Gy, media was collected at 72 h post-RT, and was subsequently isolated using Exoeasy kit as described in Materials and Methods.

As shown in Figure 4A,D, ZetaView nano tracking analysis show that the EV concentration increased (~50%) post-RT, with average EVs size being about ~150–200 nm. We further compared EV concentration and distribution of PC3 cells and clone 695 cells; as expected, clone 695 cells showed an increased in EVs concentration vs. PC3 cells (Figure 4E). As a complementary method to confirm EV release upon RT, TEM was employed (Figure 4B). Ultrastructural morphology photographs demonstrated the membrane bound vesicles of EVs from both RT versus non-RT PC3 cells (Figure 4C). These data confirm that EVs are being released from PC3 cells upon RT.

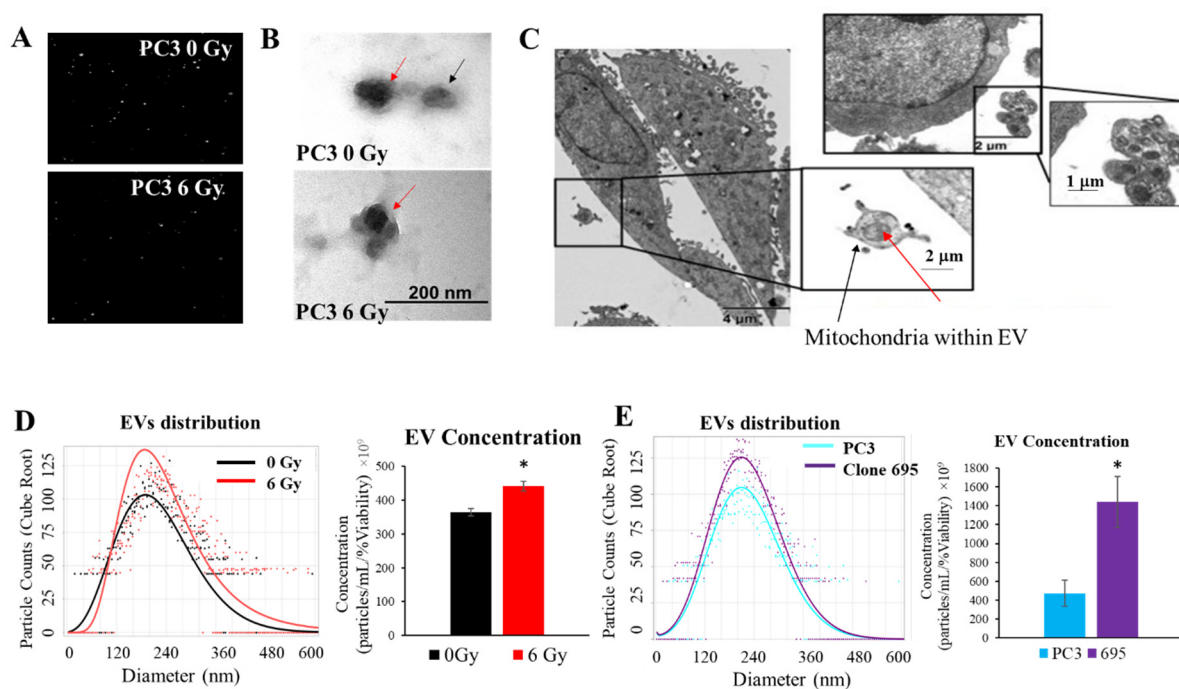


Figure 4. RT activates EVs production. (A) NTA images of particles by Zeta View Particle Matrix. (B) TEM images of EVs isolated from PC3 cells 0 Gy and 6 Gy. Red arrows denote membrane (outer gray color) and inner cargo (darker gray color). (C) EVs carrying “mitochondria-like structures” as cargo upon RT in PC3 cells. Black arrow indicates an Extracellular Vesicle and the red arrow indicates Mitochondria within the vesicles. (D) EV count and EV population isolated from PC3 cells at 0 Gy and 6 Gy. (E) EV count and distribution isolated from PC3 cells and clone 695 cells, post 72 h after seeding Margin Model from negative binomial overlaid with observed values (Predict values without random effects). * p -value < 0.05.

3.6. Extracellular Vesicles Released during Radiation Treatment Carry Mitochondria as Cargo

Since we observed the increase in mitochondrial mass and mitochondrial function in radioresistant clone 695 cells, we tested if EVs released after RT contain mitochondria. Upon EM imaging of PC3 cells subsequent to RT, it was observed that not only are EVs being released, but they also contain membranous cargo. Upon closer inspection, these membranous cargos have mitochondria-like structures (Figure 4D).

3.7. Upon Radiation Treatment, PC3 Cell Line Derived Vesicles Contained H_2O_2 -Responsive Proteins and Mitochondrial Proteins

To further identify mitochondrial components in RT-derived EVs, we measured mitochondrial proteins in EVs. Expression level for each protein was normalized to total protein loading (Supplementary Figure S4). As shown in Figure 5 upon 6 Gy RT there was an increase in both mitochondrial DNA and nuclear DNA-encoded mitochondrial proteins within RT-derived EVs. Proteins were found in these vesicles including mitochondrial protein transcription factors such as TFAM as well as mitochondrial electron transport proteins; ND4 (complex I), SDHA (complex II), and Cytochrome bc1 complex (complex III)

(Figure 5). In addition to mitochondrial proteins, it was also observed that that upon RT, there was an increase of mitochondrial H₂O₂-modifying proteins such as GPx4 and Prx3 (Figure 5). Consistently, both mitochondrial proteins and H₂O₂-responsive proteins were increased in EVs derived from PC3 cells treated with hyper fractionated RT, 2 Gy × 23 and 2 Gy × 33 (Supplementary Figure S4). The increase of these mitochondrial proteins, particularly mitochondrial antioxidants in RT-derived EVs, suggest that RT upregulates H₂O₂ production.

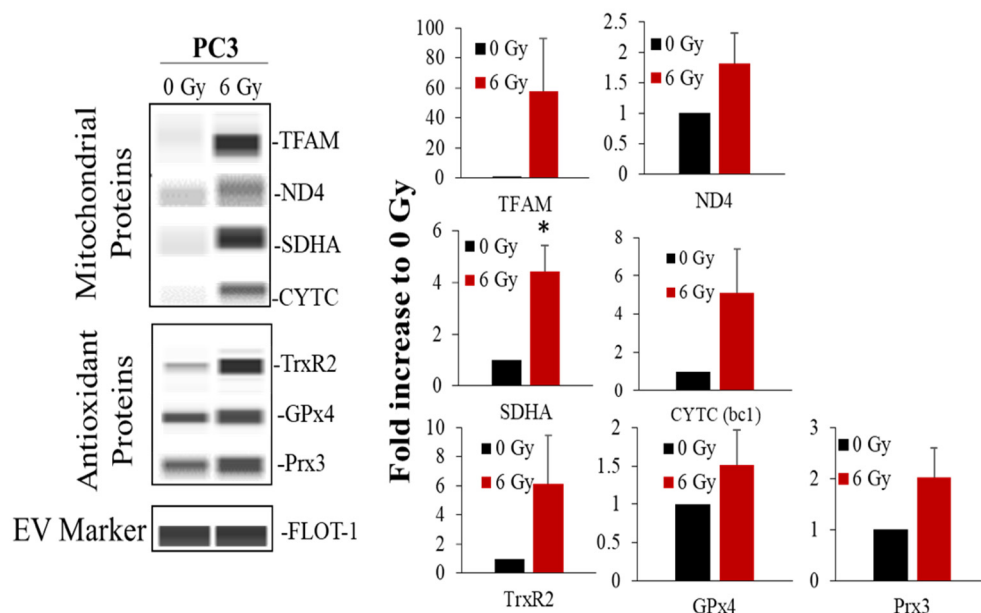


Figure 5. Upon radiation treatment, PC3 cell line derived EVs contained antioxidant and mitochondrial proteins. Mitochondrial OXPHOS proteins and H₂O₂-responsive proteins (left panel) shown in EVs derived from PC3 cells treated with 6 Gy. Bar graphs indicate average fold changes in protein expression compared to 0 Gy (from at least three separate experiments). * *p*-value < 0.05.

3.8. Radiation Induces Mitochondrial H₂O₂ Production in PC3 Cells

Due to an increase in H₂O₂ (Figure 3) in radioresistant PCa cells and the H₂O₂ responsive proteins in the RT-derived EV (Figure 5), a MitoPY1 stain was performed to determine if there was an increase in mitochondrial H₂O₂. As shown in Figure 6, there was an increase in H₂O₂ production within the mitochondria beginning around 6 h post RT and peaking at about 48–72 h post RT. These data suggest that mitochondria contributed to the H₂O₂ increased during RT of PC3 cells.

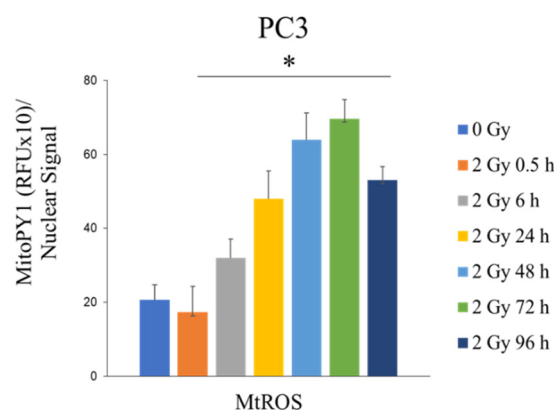


Figure 6. Increase in H₂O₂ production upon radiation treatment PC3 cells (6 Gy). H₂O₂ production in mitochondria at 0.5, 6, 24, 48, 72, and 96 h post-RT. * *p*-value < 0.05 when compared to 0 Gy.

3.9. H₂O₂ Mediates Extracellular Vesicle Release and Impairing Mitochondrial Function

Due to the production of H₂O₂ and H₂O₂-responsive proteins being released into the EVs upon RT, H₂O₂ could act as signaling molecule that mediates EV release. To test the concept, H₂O₂ (60 μM, 120 μM and 240 μM) were added to PC3 cells for 24 h and EVs were then isolated from the media. In analyzing the EVs collected from the H₂O₂ treated cells, it was observed that there was a significant increase in concentration of EVs released in the H₂O₂ treatment groups (Figure 7A). Size distribution demonstrated smaller EVs upon H₂O₂ treatment compared to the untreated control, specifically at 120 μM and 240 μM of H₂O₂. (Figure 7B). Importantly, H₂O₂-derived EVs contain an increase in mitochondrial proteins as cargo (Figure 7C), similar to RT-derived EVs (Figure 6). In performing a seahorse mitostress test, it was shown that PC3 cells had a lower OCR and spare respiratory rate, with no change in proton leak, when treated with 120 μM H₂O₂ (Figure 7D). Pre-treated PC3 cells with PEG-CAT rescued H₂O₂-mediated mitochondrial function impairment and H₂O₂-activated EV production.

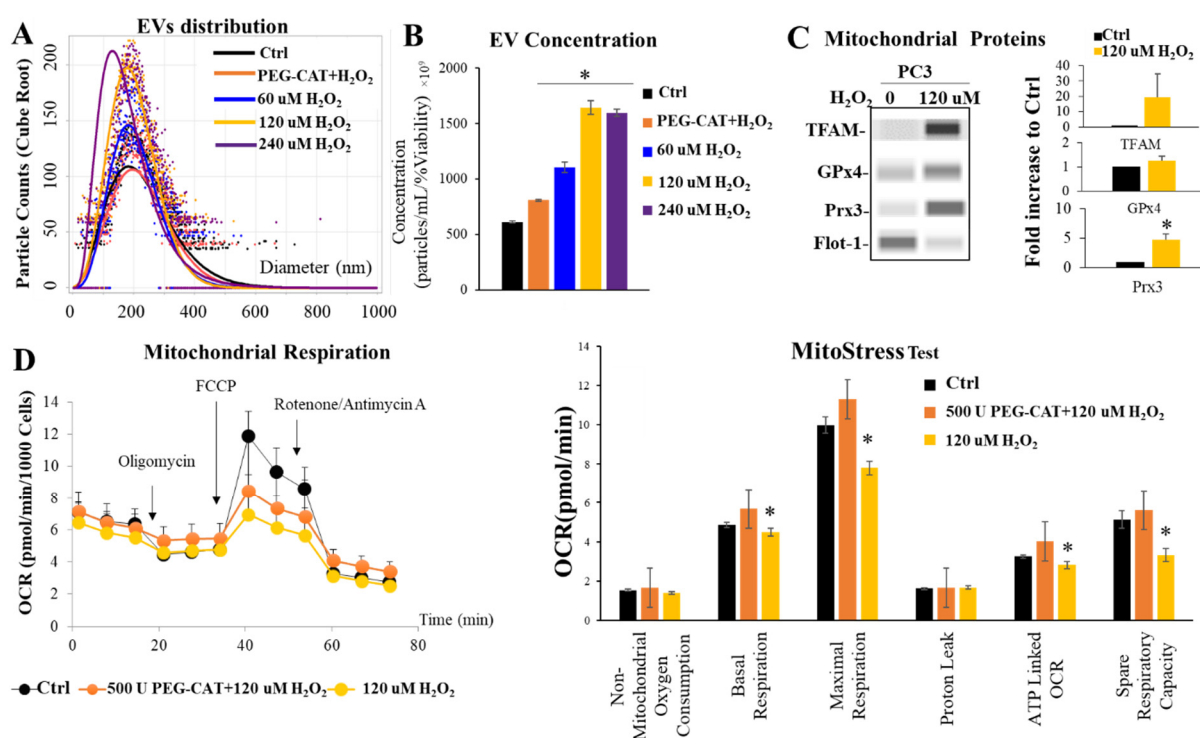


Figure 7. H₂O₂- mediated EV release and impaired mitochondrial function. (A) Size distribution of EVs derived from PC3 cells treated with H₂O₂. Margin Model from negative binomial overlaid with observed values (Predict values without random effects). (B) Concentration of EVs that derived from PC3 cells treated with H₂O₂. (C) Cargo of EVs that derived from PC3 cells treated with H₂O₂. Bar graphs indicate average fold changes in protein expression compared to control (Ctrl) (from at least three separate experiments). * *p*-value < 0.05. (D) Seahorse mitochondrial stress test of PC3 cell line after treatment of 120 μM of H₂O₂. PEG-CAT was used in combination with 120 μM H₂O₂ as control for all experiments. * *p*-value < 0.05 when compared ctrl and PEG-CAT.

3.10. Uptake of External Mitochondria Correlates with an Increase Mitochondrial Mass and Cancer Survival Post Radiation

Since an increase in mitochondria in the form of EVs were observed in PC3 cells post-RT, it was hypothesized that cells that survived RT could uptake these vesicles and utilize mitochondria to increase their chances of surviving post-RT. As shown in Figure 8A, incubation of irradiated PC3 cells with GFP labeled EVs (derived from PC3 cells treated with RT) demonstrated an uptake of EVs into the cells at around 7 h as indicated by GFP localized inside the cells (purple membrane). Quantification of EV number demonstrated

the uptake of EVs was greater observed after a 24 h incubation compared to 7 and 0 h (control). Interestingly, GFP intensity of EVs are stable between 7 and 24 h suggesting photobleaching or utilization of EVs by the recipient cells. Subsequent to EV uptake, we next tested if taking up external mitochondria would protect PC3 cells under stressed conditions. PC3 cells were pre-treated with 0 ug or 10 ug of mitochondria according to mitoception protocol [47], prior to RT (0 Gy or 2 Gy \times 3). External mitochondria were taken up by irradiated PC3 cells as early as 1.5 h as indicated by an increase in red fluorescence intensity (4 fold, Figure 8B). Subsequently, a colony survival assay was performed 10–12 days post-RT. We found that in the group treated with both radiation and mitochondria, there was a significant increase in surviving fraction when compared to the control group (0 ug of mitochondria) (Figure 8C). Overall, these data suggest that EVs can be taken up by irradiated PCa cells and acquisition of external mitochondria could potentially mediate redox reprogramming and mitochondrial homeostasis in the recipient cells for their survival and regrow after RT.

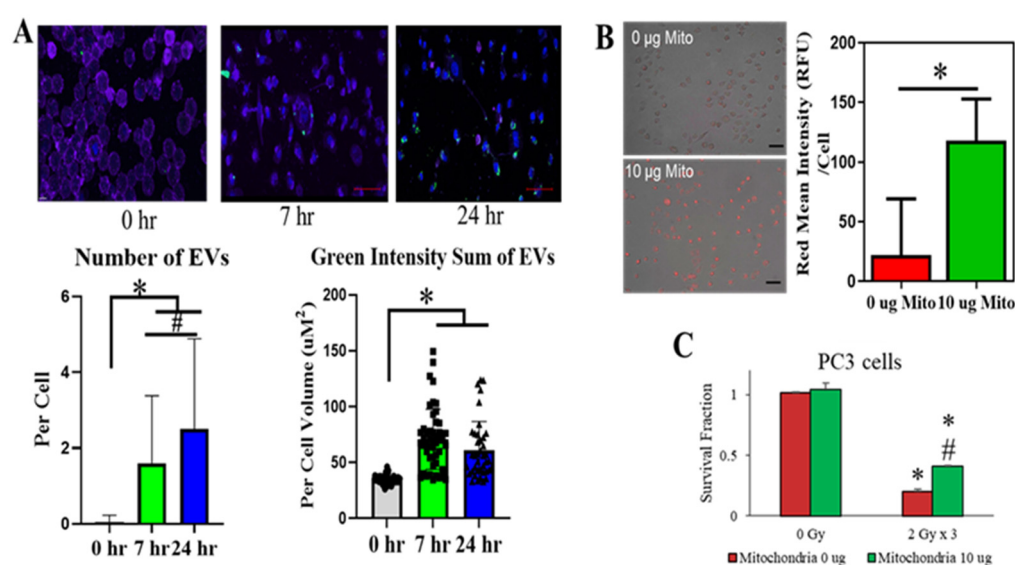


Figure 8. Uptake of mitochondria particles and increase in surviving fraction after RT in PC3 cells. (A) EV particles labeled with GFP were uptake by PC3 cells after RT. Green = EV, Purple = plasma membrane, Blue = Nucleus. Number of EVs (based on green GFP) and GFP intensity of EVs were quantify using Imaris software (* p -value < 0.0001, # p -value = 0.05). (B) Isolated external mitochondria (red) were uptake by PC3 after RT. Intensity of RFP represent amount of mitochondria in the cell. Circles, squares, and triangles represent individual data points of 0 h, 7 h, and 24 h respectively. (C) Colony survival assay of PC3 cells that uptake external mitochondria. * p -value < 0.05 when compared to 0 Gy. # p -value < 0.05 when compared to non-mitochondrial treatment.

4. Discussion

Cancer reprogramming including rewired cellular redox state, up-regulation of metabolism, and activated mitochondrial biogenesis; is an adaptive response mechanism(s) that contributes to cancer survival, cancer progression, and response to cancer therapy. Aggressive cancers have also been shown to have specific attributes, such as an increase in mitochondrial mass, ROS, and changes in mitochondrial metabolism [48–50]. We analyzed mRNA levels of mitochondrial transcription factor TFAM, which is responsible for mitochondrial biogenesis, from PCa patients with various stages ($n = 499$) compared to normal samples ($n = 52$) from The Cancer Genome Atlas (TCGA) database and found that TFAM mRNA expression levels significantly correlate with PCa Gleason scores (Gleason scores 8 > 7 > 6) (Supplementary Figure S2). Further survival analysis based on TFAM mRNA expression level (cut off at 4.71) demonstrates that PCa patients who have lower TFAM expression are likely to be disease free, when compared to PCa patients who have high TFAM expression, at >0.3 year

time frame. Overall, these data suggest that mitochondria could potentially play a role in the aggressiveness of prostate cancer and disease free PCa patients.

Mitochondria have been implicated in many cases of aggressive cancer types with an overexpression of mitochondrial cytochrome C oxidase II being involved with poor prognosis of breast cancer and frequent mitochondrial mutations in PCa [51,52]. It has also been shown that mitochondria and their DNA directly play a role in the malignant and tumorigenic transformation of PCa [53,54]. Herein, we generated clone 695 cell line to mimic cancer cells that survived and regrew after RT to test if mitochondria play role in the development of cancer resistance to RT. Upon utilization of a confocal microscope, we found that an increase in small granule structures upon RT, were most likely mitochondria (Figure 2). Increase in mitotracker green intensity indicated a higher mitochondrial mass and volume in radiation resistant cells at single cell level. Together, we hypothesize that cells with higher mitochondria are the ones that survive and become radio-resistant clone 695 cell line. In performing an Amplex red assay, TMRE stain, and MitoPY1 stain, we observed there was an increase in not only H_2O_2 released into the media, but an increase in mitochondrial membrane potential and more specifically in mitochondrial H_2O_2 of clone 695 cells compared to PC3 cells (Figure 3A). Given this data, we hypothesized that there would be an alteration of mitochondrial respiration, which is another hallmark of aggressive cancers [49,51]. In performing a seahorse mitostress test, our hypothesis was confirmed. Clone 695 cells showed a higher basal OCR, proton leak, and ATP production. Please note, the increase in mitochondrial activity could be due to an increase in mitochondrial volume per cell of clone 695 cells, not the mitochondria of clone 695 cells are more metabolically active. In fact, a higher proton leak in clone 695 cells, suggesting the mitochondria within these cells are uncoupled and oxygen consumption is being used for processes other than ATP production. This is also consistent with in the finding that clone 695 cell line has a significantly lower spare respiratory capacity. These results suggest that clone 695 cell line is functioning at maximum and cannot convert to another source of ATP as easily as PC3 cells. Increased non-mitochondrial OCR has been attributed to NADPH oxidases within the cell. Specifically for PCa, NOX 1, NOX 2, and NOX 5 have been implicated in the increase of non-mitochondrial OCR [52,55]. The glycolytic stress test and lactate measurements are not significantly different (Figure 3B) between PC3 cells and clone 695 cells. Hence, PCa does not conform to the typical Warburg effect, which is the preference of glycolysis over other processes such as the TCA cycle in even the presence of oxygen [56]. Together, the elevation of mitochondrial function in clone 695 cells is accompanied by an increase in mitochondrial H_2O_2 production, mitochondrial membrane potential, and mitochondrial mass. These data suggest that reprogramming of PCa's mitochondrial homeostasis could allow the cancer to survive and regrow after RT.

H_2O_2 is a ROS that works as a signal transduction molecule throughout the cell. One of the ways that this occurs is by reacting with thiol group or cysteines of neighboring proteins [57]. During RT, the superoxide radical is converted into H_2O_2 by proteins such as MnSOD [58]. It has been shown by Matsumito et al. that the amount of H_2O_2 produced during RT is around 0.1 to 0.25 $\mu\text{mol/L/Gy}$ [59]. Likewise, the amount of H_2O_2 that diffuses into the cell at 120 μM is estimated to be 20–35 pM [60]. This allows us to determine the effects of H_2O_2 in RT and its role in the production of EVs. EVs are produced through a process called biogenesis. This occurs by either the fusion of the vesicle with the plasma membrane or a multivesicular endosomes (MVEs) [61]. Several studies demonstrated that EVs play an important role for intercellular communication by eliminating toxic molecules from the cells, exchanging cargo between the cells, delivering cargo to the recipient cells, and activate signaling transduction in the recipient cells. We demonstrated that Clone 695 cells produce more EVs than PC3 cells and since clone 695 cells have a higher level of H_2O_2 , thus H_2O_2 may contribute to EV production. As shown in Figure 7, upon H_2O_2 treatment, EV production is increased with increasing dose of H_2O_2 . This data suggests that EVs release is at least, in part, mediated by H_2O_2 . We posit that H_2O_2 creates oxidative imbalances causing the cell to release the vesicles to remove damaged biomolecules such

as proteins or carry cargo for cell survival such as mitochondria. It is established in squamous head and neck cancer that not only the cargo of EVs are altered upon RT but these cargo promote migration of recipient cells through promoting chemotaxis induced motility as well as AKT-dependent migration [62,63]. EVs have also shown to mediate therapy resistance by regulation of DNA repair, apoptosis, and the cell cycle within recipient cells [64]. Importantly, Jang et al. have shown that EVs containing mitochondrial proteins were released in melanoma [65]. Guescini et al. demonstrated the presence of mtDNA within exosomes released by astrocytes and glioblastoma cells [62]. Similarly, we observed the EVs released upon RT also contained mitochondrial proteins and antioxidant proteins, particularly H₂O₂-responsive proteins (Figure 5, Supplementary Figure S4). The increase of these mitochondrial proteins in RT-derived EVs suggest that RT promotes H₂O₂ production, which in turn could stimulate an increase in EV release. We propose that upregulation of H₂O₂ during RT cause mitochondrial respiratory impairment which subsequently mediates EV production with mitochondria as a cargo to maintain mitochondrial quality control by removing damaged mitochondria or deliver mitochondrial contents to recipient cells [63]. More importantly, alteration of mitochondrial respiratory function could further promote mitochondrial H₂O₂ production which can be transported across mitochondrial membrane to endoplasmic reticulum via aquaporin 11, allowing redox signal conduct in cytoplasm [66] such as activation of calmodulin-dependent protein kinase kinase (CaMKK) [67], which is responsible for MVE formation [64,68]. Please note, in addition to mitochondria or mitochondrial proteins as cargo, RT-derived EVs could carry miRNA, DNA, cytokines, and other transcription factors; which are not being discussed since they are beyond the scope of this study. Moreover, van der Pol et al., as well as Erdbürgger and Lannigan, showed that different methods of EV analysis and isolation can determine the observable size of these vesicles [69,70]. Despite the sensitivity of TEM's region selection, sample preparations, and the setting of NTA instrument (not exceed 1000 nm), smaller size EVs (~200 nm) that contain "mitochondria-like structures" have not yet been observed by TEM. For the purpose of this paper in terms of what the EVs are carrying, as long as they contain mitochondrial contents or "mitochondria-like structures", they will be our subject of interest.

Despite these findings and many others, the mechanisms of how mitochondria are packaged in the EVs and how EVs carrying mitochondrial contents are being utilized by recipient PCa cells for possible repair and survival is mostly unknown [71]. A probable mechanism of action could involve the antioxidants carried within the EVs, activating their anti-stress defense systems as demonstrated by Kahroba et al. [72]. Moreover, release of mitochondrial ROS in the cytosol has been show to induce the changes of gene expression through activation of calcineurin and the Cn-dependent retrograde signaling pathway [73], release metabolites to induce histone acetylation [74], and regulate mitochondrial metabolism (mitochondrial fission and fusion) through AMPK activation [75,76]. Here, in, we propose that these vesicles can be taken up by endocytosis in other (recipient) cells and the recipient cells then utilize these vesicles containing mitochondria to produce ATP, to provide precursors of cellular metabolism, to elevate mitochondrial metabolism and to rewire cellular redox state, which are characteristics observed in PCa that survives RT.

Overall, our data suggests that that H₂O₂ promotes the production of EVs carrying mitochondrial proteins and that functional mitochondria enhance cancer survival after RT. As show in Figure 9, the increase of H₂O₂ production induced the release of EVs containing mitochondria from donor cells. These EVs containing mitochondria can then be taken up by recipient cells. Recipient cells have shown to have an increase in mitochondrial ROS, OCR, mitochondrial mass, and antioxidant proteins, which are also the shown in radioresistant PCa. Extracellular vesicles released post-RT and the cargo within them could aid in the survival of recipient cells. In conclusion, this novel cancer reprogramming phenomena, which is activated by H₂O₂, could (1) provide a better insight into therapy-induced resistant cancer's underlying mechanism; more specifically the role of mitochondria and mitochondrial transfer and (2) could serve as a target to enhance radiation treatment and prevent cancer treatment failure.

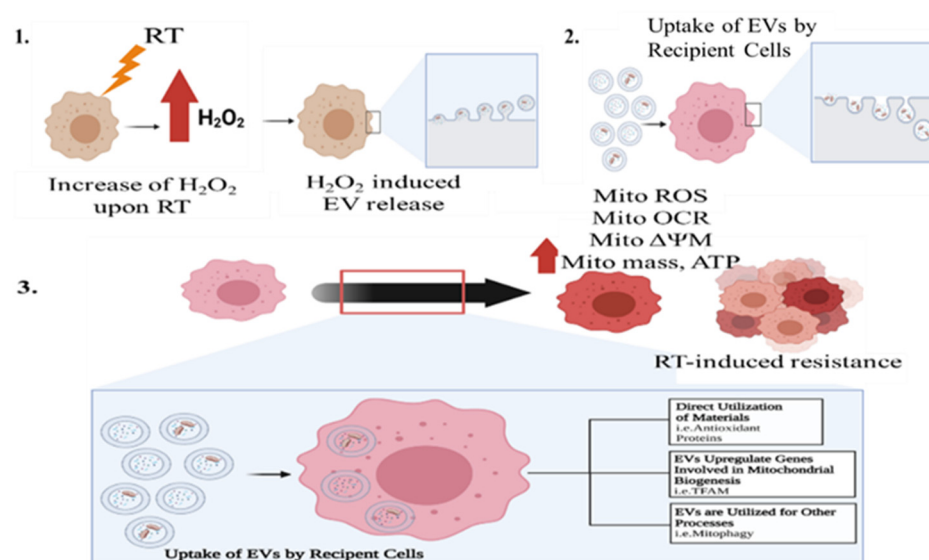


Figure 9. Proposed mechanism of how RT-derived H₂O₂ (1) Reprogram mitochondrial homeostasis in the recipient cells through EVs containing mitochondria (2), which allows the cancer to survive and regrow after RT (3).

Supplementary Materials: The following supporting information can be downloaded at: <https://www.mdpi.com/article/10.3390/antiox11112119/s1>, Figure S1: Cell line authentication (Clone 695); Figure S2. Oncomine TCGA analysis of PCa patients in varying stages of tumor progression; Figure S3: (A) Automated algorithm generated by Imaris software for segmentation of mitochondrion. (B) Individual segmented mitochondrion; Figure S4: (A) Expressions of mitochondrial proteins in EVs isolated from post-RT PC3 cells. (B) Total protein loading (1 µg/µL) of each representative sample.

Author Contributions: Conceptualization, C.E.M., L.C. and D.K.S.C.; methodology, validation, L.C., W.H.S.C. and D.K.S.C.; formal analysis, H.L.W., L.C. and C.E.M., investigation, C.E.M., L.C., F.X., Y.Z., K.M., W.Z., W.L. and H.L.W.; resources, W.H.S.C., L.C. and D.K.S.C.; data curation, C.E.M., L.C., R.J. and H.L.W.; writing—original draft preparation, C.E.M.; writing—review and editing, C.E.M. and L.C.; visualization, C.E.M.; supervision, L.C. and D.K.S.C.; funding acquisition, W.H.S.C., D.K.S.C. and L.C. All authors have read and agreed to the published version of the manuscript.

Funding: This work was supported, in part, by NIH grants R01 CA251663 (L.C.), R01 CA205400 (W.H.S.C. and D.K.S.C.), P20 GM121327 (L.C. and D.K.S.C.), and Markey Woman Strong (L.C.). Our research utilized the service facilities of the Markey Cancer Redox Metabolism and Biostatistics and Bioinformatics Shared Resource Facilities funded by a Markey Cancer Center support grant (P30 CA177558).

Institutional Review Board Statement: Not applicable.

Data Availability Statement: Not applicable.

Acknowledgments: Authors would like to thank Chi Wang and Daheng He for assistance on TCGA oncomine data analysis. Alan B Butterfield and Michael Alstott for Seahorse experiments. James Campbell for assistance in carry out a cell viability experiment. Figures 1A and 9 were created using BioRender.com.

Conflicts of Interest: The authors declare no conflict of interest.

References

1. Siegel, R.L.; Miller, K.D.; Fuchs, H.E.; Jemal, A. Cancer statistics, 2022. *CA Cancer J. Clin.* **2022**, *72*, 7–33. [[CrossRef](#)] [[PubMed](#)]
2. Xin, L. Cells of origin for cancer: An updated view from prostate cancer. *Oncogene* **2013**, *32*, 3655–3663. [[CrossRef](#)]
3. Society, A.C. *Cancer Facts & Figures 2022*; American Cancer Society: Atlanta, GA, USA, 2022.
4. Siegel, R.L.; Miller, K.D.; Fuchs, H.E.; Jemal, A. Cancer Statistics, 2021. *CA Cancer J. Clin.* **2021**, *71*, 7–33. [[CrossRef](#)]
5. Siegel, R.L.; Miller, K.D.; Jemal, A. Cancer statistics, 2020. *CA Cancer J. Clin.* **2020**, *70*, 7–30. [[CrossRef](#)]

6. Prostate Cancer Treatment (PDQ(R)). Patient Version. In *PDQ Cancer Information Summaries*; Prostate Cancer Treatment (PDQ(R)): Bethesda, MD, USA, 2002.
7. Holley, A.K.; Miao, L.; St Clair, D.K.; St Clair, W.H. Redox-modulated phenomena and radiation therapy: The central role of superoxide dismutases. *Antioxid. Redox Signal.* **2014**, *20*, 1567–1589. [[CrossRef](#)] [[PubMed](#)]
8. Baskar, R.; Dai, J.; Wenlong, N.; Yeo, R.; Yeoh, K.W. Biological response of cancer cells to radiation treatment. *Front. Mol. Biosci.* **2014**, *1*, 24. [[CrossRef](#)]
9. Kim, W.; Lee, S.; Seo, D.; Kim, D.; Kim, K.; Kim, E.; Kang, J.; Seong, K.M.; Youn, H.; Youn, B. Cellular Stress Responses in Radiotherapy. *Cells* **2019**, *8*, 1105. [[CrossRef](#)]
10. Chaiswing, L.; Weiss, H.L.; Jayswal, R.D.; Clair, D.K.S.; Kyprianou, N. Profiles of Radioresistance Mechanisms in Prostate Cancer. *Crit. Rev. Oncog.* **2018**, *23*, 39–67. [[CrossRef](#)]
11. Kulkarni, R.; Marples, B.; Balasubramaniam, M.; Thomas, R.A.; Tucker, J.D. Mitochondrial gene expression changes in normal and mitochondrial mutant cells after exposure to ionizing radiation. *Radiat. Res.* **2010**, *173*, 635–644. [[CrossRef](#)] [[PubMed](#)]
12. Cloos, C.R.; Daniels, D.H.; Kalen, A.; Matthews, K.; Du, J.; Goswami, P.C.; Cullen, J.J. Mitochondrial DNA depletion induces radioresistance by suppressing G2 checkpoint activation in human pancreatic cancer cells. *Radiat. Res.* **2009**, *171*, 581–587. [[CrossRef](#)]
13. Gough, D.R.; Cotter, T.G. Hydrogen peroxide: A Jekyll and Hyde signalling molecule. *Cell Death Dis.* **2011**, *2*, e213. [[CrossRef](#)] [[PubMed](#)]
14. Bienert, G.P.; Schjoerring, J.K.; Jahn, T.P. Membrane transport of hydrogen peroxide. *Biochim. Biophys. Acta (BBA)-Biomembr.* **2006**, *1758*, 994–1003. [[CrossRef](#)] [[PubMed](#)]
15. Laporte, A.; Lortz, S.; Schaal, C.; Lenzen, S.; Elsner, M. Hydrogen peroxide permeability of cellular membranes in insulin-producing cells. *Biochim. Biophys. Acta (BBA)-Biomembr.* **2020**, *1862*, 183096. [[CrossRef](#)] [[PubMed](#)]
16. Rubio, C.; Cerón, J. Spectrophotometric assays for evaluation of Reactive Oxygen Species (ROS) in serum: General concepts and applications in dogs and humans. *BMC Vet. Res.* **2021**, *17*, 226. [[CrossRef](#)] [[PubMed](#)]
17. Ledo, A.; Fernandes, E.; Salvador, A.; Laranjinha, J.; Barbosa, R.M. In vivo hydrogen peroxide diffusivity in brain tissue supports volume signaling activity. *Redox Biol.* **2022**, *50*, 102250. [[CrossRef](#)]
18. Chaiswing, L.; St Clair, W.H.; St Clair, D.K. Redox Paradox: A Novel Approach to Therapeutics-Resistant Cancer. *Antioxid. Redox Signal.* **2018**, *29*, 1237–1272. [[CrossRef](#)]
19. Sies, H. Hydrogen peroxide as a central redox signaling molecule in physiological oxidative stress: Oxidative eustress. *Redox Biol.* **2017**, *11*, 613–619. [[CrossRef](#)] [[PubMed](#)]
20. Jones, D.P.; Sies, H. The Redox Code. *Antioxid. Redox Signal.* **2015**, *23*, 734–746. [[CrossRef](#)] [[PubMed](#)]
21. Lisanti, M.P.; Martinez-Outschoorn, U.E.; Lin, Z.; Pavlides, S.; Whitaker-Menezes, D.; Pestell, R.G.; Howell, A.; Sotgia, F. Hydrogen peroxide fuels aging, inflammation, cancer metabolism and metastasis: The seed and soil also needs “fertilizer”. *Cell Cycle* **2011**, *10*, 2440–2449. [[CrossRef](#)]
22. Averbeck, D.; Rodriguez-Lafrasse, C. Role of Mitochondria in Radiation Responses: Epigenetic, Metabolic, and Signaling Impacts. *Int. J. Mol. Sci.* **2021**, *22*, 11047. [[CrossRef](#)]
23. Rossmann, M.P.; Dubois, S.M.; Agarwal, S.; Zon, L.I. Mitochondrial function in development and disease. *Dis. Model. Mech.* **2021**, *14*, dmm048912. [[CrossRef](#)]
24. Brand, M.D. Mitochondrial generation of superoxide and hydrogen peroxide as the source of mitochondrial redox signaling. *Free Radic. Biol. Med.* **2016**, *100*, 14–31. [[CrossRef](#)]
25. Murphy, M.P. How mitochondria produce reactive oxygen species. *Biochem. J.* **2009**, *417*, 1–13. [[CrossRef](#)]
26. Guo, C.; Sun, L.; Chen, X.; Zhang, D. Oxidative stress, mitochondrial damage and neurodegenerative diseases. *Neural Regen. Res.* **2013**, *8*, 2003–2014. [[CrossRef](#)]
27. Jornayvaz, F.R.; Shulman, G.I. Regulation of mitochondrial biogenesis. *Essays Biochem.* **2010**, *47*, 69–84. [[CrossRef](#)]
28. Liu, D.; Gao, Y.; Liu, J.; Huang, Y.; Yin, J.; Feng, Y.; Shi, L.; Meloni, B.P.; Zhang, C.; Zheng, M.; et al. Intercellular mitochondrial transfer as a means of tissue revitalization. *Signal Transduct. Target. Ther.* **2021**, *6*, 65. [[CrossRef](#)]
29. Liu, Z.; Sun, Y.; Qi, Z.; Cao, L.; Ding, S. Mitochondrial transfer/transplantation: An emerging therapeutic approach for multiple diseases. *Cell Biosci.* **2022**, *12*, 66. [[CrossRef](#)]
30. Raposo, G.; Stoorvogel, W. Extracellular vesicles: Exosomes, microvesicles, and friends. *J. Cell Biol.* **2013**, *200*, 373–383. [[CrossRef](#)]
31. Yanez-Mo, M.; Siljander, P.R.; Andreu, Z.; Zavec, A.B.; Borrás, F.E.; Buzas, E.I.; Buzas, K.; Casal, E.; Cappello, F.; Carvalho, J.; et al. Biological properties of extracellular vesicles and their physiological functions. *J. Extracell. Vesicles* **2015**, *4*, 27066. [[CrossRef](#)]
32. Doyle, L.M.; Wang, M.Z. Overview of Extracellular Vesicles, Their Origin, Composition, Purpose, and Methods for Exosome Isolation and Analysis. *Cells* **2019**, *8*, 727. [[CrossRef](#)]
33. Borges, F.T.; Reis, L.A.; Schor, N. Extracellular vesicles: Structure, function, and potential clinical uses in renal diseases. *Braz. J. Med. Biol. Res.* **2013**, *46*, 824–830. [[CrossRef](#)]
34. Bapst, A.M.; Knöpfel, T.; Nolan, K.A.; Imeri, F.; Schuh, C.D.; Hall, A.M.; Guo, J.; Katschinski, D.M.; Wenger, R.H. Neurogenic and pericytic plasticity of conditionally immortalized cells derived from renal erythropoietin-producing cells. *J. Cell. Physiol.* **2022**, *237*, 2420–2433. [[CrossRef](#)]
35. Amari, L.; Germain, M. Mitochondrial Extracellular Vesicles—Origins and Roles. *Front. Mol. Neurosci.* **2021**, *14*, 767219. [[CrossRef](#)]

36. O'Brien, K.; Ughetto, S.; Mahjoun, S.; Nair, A.V.; Breakefield, X.O. Uptake, functionality, and re-release of extracellular vesicle-encapsulated cargo. *Cell Rep.* **2022**, *39*, 110651. [[CrossRef](#)]
37. Ramirez-Garrastacho, M.; Bajo-Santos, C.; Line, A.; Martens-Uzunova, E.S.; de la Fuente, J.M.; Moros, M.; Soekmadji, C.; Tasken, K.A.; Llorente, A. Extracellular vesicles as a source of prostate cancer biomarkers in liquid biopsies: A decade of research. *Br. J. Cancer* **2022**, *126*, 331–350. [[CrossRef](#)]
38. Gaglani, S.; Gonzalez-Kozlova, E.; Lundon, D.J.; Tewari, A.K.; Dogra, N.; Kyprianou, N. Exosomes as A Next-Generation Diagnostic and Therapeutic Tool in Prostate Cancer. *Int. J. Mol. Sci.* **2021**, *22*, 10131. [[CrossRef](#)]
39. Chen, T.Y.; Gonzalez-Kozlova, E.; Soleymani, T.; La Salvia, S.; Kyprianou, N.; Sahoo, S.; Tewari, A.K.; Cordon-Cardo, C.; Stolovitzky, G.; Dogra, N. Extracellular vesicles carry distinct proteo-transcriptomic signatures that are different from their cancer cell of origin. *iScience* **2022**, *25*, 104414. [[CrossRef](#)]
40. Chaiswing, L.; Yarana, C.; St. Clair, W.; Tovmasyan, A.; Batinic-Haberle, I.; Spasojevic, I.; St. Clair, D. A Redoxable Mn Porphyrin, MnTnBuOE-2-PyP⁵⁺, Synergizes with Carboplatin in Treatment of Chemoresistant Ovarian Cell Line. *Oxidative Med. Cell. Longev.* **2022**, *2022*, 9664636. [[CrossRef](#)]
41. Chaiswing, L.; Zhong, W.; Oberley, T.D. Increasing discordant antioxidant protein levels and enzymatic activities contribute to increasing redox imbalance observed during human prostate cancer progression. *Free Radic. Biol. Med.* **2014**, *67*, 342–352. [[CrossRef](#)]
42. Indo, H.P.; Ito, H.; Nakagawa, K.; Chaiswing, L.; Majima, H.J. Translocation of HSP47 and generation of mitochondrial reactive oxygen species in human neuroblastoma SK-N-SH cells following electron and X-ray irradiation. *Arch. Biochem. Biophys.* **2021**, *703*, 108853. [[CrossRef](#)]
43. Wei, X.; Xu, Y.; Xu, F.F.; Chaiswing, L.; Schnell, D.; Noel, T.; Wang, C.; Chen, J.; St Clair, D.K.; St Clair, W.H. RelB Expression Determines the Differential Effects of Ascorbic Acid in Normal and Cancer Cells. *Cancer Res.* **2017**, *77*, 1345–1356. [[CrossRef](#)]
44. Franken, N.A.P.; Rodermond, H.M.; Stap, J.; Haveman, J.; van Bree, C. Clonogenic assay of cells in vitro. *Nat. Protoc.* **2006**, *1*, 2315–2319. [[CrossRef](#)]
45. Tian, Y.; Gong, M.; Hu, Y.; Liu, H.; Zhang, W.; Zhang, M.; Hu, X.; Aubert, D.; Zhu, S.; Wu, L.; et al. Quality and efficiency assessment of six extracellular vesicle isolation methods by nano-flow cytometry. *J. Extracell. Vesicles* **2020**, *9*, 1697028. [[CrossRef](#)]
46. Bourdeau-Heller, J.; Oberley, T.D. Prostate carcinoma cells selected by long-term exposure to reduced oxygen tension show remarkable biochemical plasticity via modulation of superoxide, HIF-1 α levels, and energy metabolism. *J. Cell. Physiol.* **2007**, *212*, 744–752. [[CrossRef](#)]
47. Caicedo, A.; Fritz, V.; Brondello, J.-M.; Ayala, M.; Dennemont, I.; Abdellaoui, N.; de Fraipont, F.; Moisan, A.; Prouteau, C.A.; Boukhaddaoui, H.; et al. MitoCeption as a new tool to assess the effects of mesenchymal stem/stromal cell mitochondria on cancer cell metabolism and function. *Sci. Rep.* **2015**, *5*, 9073. [[CrossRef](#)]
48. Farnie, G.; Sotgia, F.; Lisanti, M.P. High mitochondrial mass identifies a sub-population of stem-like cancer cells that are chemo-resistant. *Oncotarget* **2015**, *6*, 30472–30486. [[CrossRef](#)]
49. McCann, E.; O'Sullivan, J.; Marcone, S. Targeting cancer-cell mitochondria and metabolism to improve radiotherapy response. *Transl. Oncol.* **2021**, *14*, 100905. [[CrossRef](#)]
50. Liu, Y.e.; Shi, Y. Mitochondria as a target in cancer treatment. *MedComm* **2020**, *1*, 129–139. [[CrossRef](#)]
51. Kumar, P.R.; Moore, J.A.; Bowles, K.M.; Rushworth, S.A.; Moncrieff, M.D. Mitochondrial oxidative phosphorylation in cutaneous melanoma. *Br. J. Cancer* **2021**, *124*, 115–123. [[CrossRef](#)]
52. Holl, M.; Koziel, R.; Schafer, G.; Pircher, H.; Pauck, A.; Hermann, M.; Klocker, H.; Jansen-Durr, P.; Sampson, N. ROS signaling by NADPH oxidase 5 modulates the proliferation and survival of prostate carcinoma cells. *Mol. Carcinog.* **2016**, *55*, 27–39. [[CrossRef](#)]
53. Vayalil, P.K. Mitochondrial oncoenergetics of prostate tumorigenesis (Review). *Oncol. Lett.* **2019**, *18*, 4367–4376. [[CrossRef](#)] [[PubMed](#)]
54. Petros, J.A.; Baumann, A.K.; Ruiz-Pesini, E.; Amin, M.B.; Sun, C.Q.; Hall, J.; Lim, S.; Issa, M.M.; Flanders, W.D.; Hosseini, S.H.; et al. mtDNA mutations increase tumorigenicity in prostate cancer. *Proc. Natl. Acad. Sci. USA* **2005**, *102*, 719–724. [[CrossRef](#)] [[PubMed](#)]
55. Sun, Y.; St Clair, D.K.; Xu, Y.; Crooks, P.A.; St Clair, W.H. A NADPH oxidase-dependent redox signaling pathway mediates the selective radiosensitization effect of parthenolide in prostate cancer cells. *Cancer Res.* **2010**, *70*, 2880–2890. [[CrossRef](#)] [[PubMed](#)]
56. Eidelman, E.; Twum-Ampofo, J.; Ansari, J.; Siddiqui, M.M. The Metabolic Phenotype of Prostate Cancer. *Front. Oncol.* **2017**, *7*, 131. [[CrossRef](#)]
57. Lennicke, C.; Rahn, J.; Lichtenfels, R.; Wessjohann, L.A.; Seliger, B. Hydrogen peroxide–production, fate and role in redox signaling of tumor cells. *Cell Commun. Signal.* **2015**, *13*, 39. [[CrossRef](#)]
58. Candas, D.; Li, J.J. MnSOD in oxidative stress response-potential regulation via mitochondrial protein influx. *Antioxid. Redox Signal.* **2014**, *20*, 1599–1617. [[CrossRef](#)]
59. Matsumoto, K.I.; Ueno, M.; Nyui, M.; Shoji, Y.; Nakanishi, I. Effects of LET on oxygen-dependent and-independent generation of hydrogen peroxide in water irradiated by carbon-ion beams. *Free Radic. Res.* **2021**, *55*, 714–719. [[CrossRef](#)]
60. Wagner, B.A.; Evig, C.B.; Reszka, K.J.; Buettner, G.R.; Burns, C.P. Doxorubicin increases intracellular hydrogen peroxide in PC3 prostate cancer cells. *Arch. Biochem. Biophys.* **2005**, *440*, 181–190. [[CrossRef](#)]
61. Abels, E.R.; Breakefield, X.O. Introduction to Extracellular Vesicles: Biogenesis, RNA Cargo Selection, Content, Release, and Uptake. *Cell. Mol. Neurobiol.* **2016**, *36*, 301–312. [[CrossRef](#)]

62. Guescini, M.; Genedani, S.; Stocchi, V.; Agnati, L.F. Astrocytes and Glioblastoma cells release exosomes carrying mtDNA. *J. Neural Transm.* **2010**, *117*, 1–4. [[CrossRef](#)]
63. Zhang, Y.; Tan, J.; Miao, Y.; Zhang, Q. The effect of extracellular vesicles on the regulation of mitochondria under hypoxia. *Cell Death Dis.* **2021**, *12*, 358. [[CrossRef](#)] [[PubMed](#)]
64. Stewart, L.M.; Gerner, L.; Rettel, M.; Stein, F.; Burrows, J.F.; Mills, I.G.; Evergren, E. CaMKK2 facilitates Golgi-associated vesicle trafficking to sustain cancer cell proliferation. *Cell Death Dis.* **2021**, *12*, 1040. [[CrossRef](#)] [[PubMed](#)]
65. Jang, S.C.; Crescitelli, R.; Cvjetkovic, A.; Belgrano, V.; Olofsson Bagge, R.; Sundfeldt, K.; Ochiya, T.; Kalluri, R.; Lotvall, J. Mitochondrial protein enriched extracellular vesicles discovered in human melanoma tissues can be detected in patient plasma. *J. Extracell. Vesicles* **2019**, *8*, 1635420. [[CrossRef](#)] [[PubMed](#)]
66. Sorrentino, I.; Galli, M.; Medrano-Fernandez, I.; Sitia, R. Transfer of H₂O₂ from Mitochondria to the endoplasmic reticulum via Aquaporin-11. *Redox Biol.* **2022**, *55*, 102410. [[CrossRef](#)] [[PubMed](#)]
67. Takata, T.; Kimura, J.; Ihara, H.; Hatano, N.; Tsuchiya, Y.; Watanabe, Y. Redox regulation of Ca(2+)/calmodulin-dependent protein kinase IV via oxidation of its active-site cysteine residue. *Free Radic. Biol. Med.* **2019**, *130*, 99–106. [[CrossRef](#)]
68. Ariotti, N.; Wu, Y.; Okano, S.; Gambin, Y.; Follett, J.; Rae, J.; Ferguson, C.; Teasdale, R.D.; Alexandrov, K.; Meunier, F.A.; et al. An inverted CAV1 (caveolin 1) topology defines novel autophagy-dependent exosome secretion from prostate cancer cells. *Autophagy* **2021**, *17*, 2200–2216. [[CrossRef](#)]
69. van der Pol, E.; Coumans, F.A.W.; Grootemaat, A.E.; Gardiner, C.; Sargent, I.L.; Harrison, P.; Sturk, A.; van Leeuwen, T.G.; Nieuwland, R. Particle size distribution of exosomes and microvesicles determined by transmission electron microscopy, flow cytometry, nanoparticle tracking analysis, and resistive pulse sensing. *J. Thromb. Haemost.* **2014**, *12*, 1182–1192. [[CrossRef](#)]
70. Erdbrügger, U.; Lannigan, J. Analytical challenges of extracellular vesicle detection: A comparison of different techniques. *Cytom. Part A* **2016**, *89*, 123–134. [[CrossRef](#)]
71. He, D.; Zhao, Z.; Fu, B.; Li, X.; Zhao, L.; Chen, Y.; Liu, L.; Liu, R.; Li, J. Exosomes Participate in the Radiotherapy Resistance of Cancers. *Radiat Res.* **2022**, *Online ahead of print*. [[CrossRef](#)]
72. Kahroba, H.; Davatgaran-Taghipour, Y. Exosomal Nrf2: From anti-oxidant and anti-inflammation response to wound healing and tissue regeneration in aged-related diseases. *Biochimie* **2020**, *171–172*, 103–109. [[CrossRef](#)]
73. Chowdhury, A.R.; Zielonka, J.; Kalyanaraman, B.; Hartley, R.C.; Murphy, M.P.; Avadhani, N.G. Mitochondria-targeted paraquat and metformin mediate ROS production to induce multiple pathways of retrograde signaling: A dose-dependent phenomenon. *Redox Biol.* **2020**, *36*, 101606. [[CrossRef](#)]
74. Corbet, C.; Pinto, A.; Martherus, R.; Santiago de Jesus, J.P.; Polet, F.; Feron, O. Acidosis Drives the Reprogramming of Fatty Acid Metabolism in Cancer Cells through Changes in Mitochondrial and Histone Acetylation. *Cell Metab.* **2016**, *24*, 311–323. [[CrossRef](#)] [[PubMed](#)]
75. Herzig, S.; Shaw, R.J. AMPK: Guardian of metabolism and mitochondrial homeostasis. *Nat. Rev. Mol. Cell Biol.* **2018**, *19*, 121–135. [[CrossRef](#)] [[PubMed](#)]
76. Garcia-Roves, P.M.; Osler, M.E.; Holmstrom, M.H.; Zierath, J.R. Gain-of-function R225Q mutation in AMP-activated protein kinase gamma3 subunit increases mitochondrial biogenesis in glycolytic skeletal muscle. *J. Biol. Chem.* **2008**, *283*, 35724–35734. [[CrossRef](#)] [[PubMed](#)]